Mass Transfer and Electrochemical Kinetic Interactions in Localized Pitting Corrosion

Identification and characterization of coupled diffusional and electrochemical kinetics effects was achieved under potentiostatic anodic dissolution conditions. A one-dimensional artificial pit geometry with sample wire electrodes embedded in an inert support exposed to NaCl solutions was used to study the dissolution of stainless steel and high-nickel Alloy 600. Multiple steady states for both materials were determined at conditions where the diffusional transport rates balanced the electrochemical rate of dissolution at the surface of the wire electrode. A theoretical transport model was developed to quantitatively explain the observed multiple steady state phenomena.

G. T. Gaudet, W. T. Mo, T. A. Hatton, J. W. Tester, J. Tilly
Massachusetts Institute of Technology
School of Chemical Engineering Practice
Brookhaven National Laboratory

H. S. Isaacs, R. C. Newman
Department of Nuclear Engineering
Brookhaven National Laboratory
Upton, NY 11973

SCOPE

Coupling of the rates of mass transfer and chemical reaction is common in systems of interest to chemical engineers. One example of this occurs in pitting corrosion. In the presence of chloride ions, pitting corrosion of alloys such as stainless steel occurs only when the electrochemical potential exceeds a minimum value called the critical pitting potential. Tester and Isaacs (1975) and Beck (1973) suggested that the corrosion rate in this range of potential is possibly controlled by the diffusion rate of metal ions out of the pit, since the true metal dissolution rate is much faster. Diffusion control was experimentally verified for potentiostatic conditions above the critical pitting potential using a one-dimensional artificial pit consisting of a metal wire mounted in an inert support with its top surface exposed to a stagnant chloride solution.

In later experiments by Newman and Isaacs (1983), the potential of an artificial pit undergoing quasi-steady dissolution was suddenly lowered to below the critical value. The dissolution rate was thereby reduced, and diffusion was no longer the single rate-limiting process. The observed rapid decline in current after a short induction period at the lower potential suggested the possible existence of multiple steady states where the rates of diffusion and metal dissolution reaction were balanced.

In this work, the transient coupling of diffusion and electrochemical reaction were examined, both theoretically and experimentally, to verify the existence of multiple steady states of pitting corrosion, where different current densities (metal dissolution rates or corrosion rates) occur under the same operating conditions.

CONCLUSIONS AND SIGNIFICANCE

By imposing a potential step change on a wire electrode exposed to a 1 mol/L sodium chloride solution, current-time data were collected; these data were then reduced using a diffusion model. The results show that at the higher potentials metal ion diffusion is adequately described by Fick's law with a single effective diffusivity, in which the effects of ion concentration on the diffusion coefficient and electromigration under a potential gradient are taken into account. The current-time data were also corrected for the effect of electrical resistance changes in the pit as the wire dissolved and the diffusion length increased. These analyses allowed the current-time decay curves obtained at different pit depths to be reduced to a single isopotential line with a maximum error of only 7% of the peak value.

The measured values of the current density correspond to the effective dissolution rate of the metal. For

a given potential step change, the measured current-time data were translated into a set of current-surface concentration plots with the aid of the diffusion model. In these diagrams, the diffusion rate was observed to be linear in accordance with Fick's law. The intersections of the diffusion line with the isopotential line obtained above should predict the location of the stable and unstable steady states.

Experimental values of the minimum pit depth at which steady state dissolution was reached were about 20% smaller than values estimated from isopotential data. Moreover, the values of the current density observed at steady state were higher than predicted. These discrepancies can be explained qualitatively by an increase in the surface area of the wire and local regions of high metal chloride concentration caused by nonuniform dissolution.

Background

Localized pitting corrosion is a major problem in the chemical process industry. Stainless steel and other alloys containing iron, chromium, and nickel in varying amounts are usually covered by a film of metal oxides that protect the metal surface from dissolving. When exposed to environments containing aggressive chloride anions, however, the passive oxide layer is undermined. Chloride ions penetrate the oxide layer at specific points on the surface, and increase the rate at which metal dissolves by the reaction: $M \rightarrow M^{n+} + ne^-$. This reaction leads to a current flow from the pit (anode) to the nearby metal surface (cathode), which remains passive. The creation of this local anode site causes a continued buildup of chloride ions as well as a decrease in pH due to hydrolysis of the metal ions. This increase in chloride concentration and decrease in pH prevents repassivation of the metal surface. Metal dissolution due to pitting as described above initiates only when a particular electrochemical potential is exceeded (Galvele, 1976). The value of this potential is called the critical pitting potential.

Tester and Isaacs (1975) have studied the interaction of reaction and diffusion in the pitting corrosion of stainless steel. In a typical experiment, a constant potential above the critical pitting potential was maintained on a 1 mm dia. wire electrode mounted in Teflon or epoxy to provide a one-dimensional artificial corrosion pit with inert side walls. The surface of the wire was exposed to an aqueous solution, usually concentrated chlorides (NaCl, HCl, $FeCl_2$, $NiCl_2$, $CuCl_2$, etc.), and as the metal corroded or dissolved it receded into the support and increased the diffusion length. When the depth was approximately 0.1 cm, a substantial concentration gradient (about 40 mol/L · cm) was sustained within the artificial pit from a saturated, near-saturated, or even supersaturated concentration of metal chlorides at the metal-solution interface to the bulk concentration outside the diffusional boundary layer. At high enough applied potential (greater than 100 millivolts relative to the saturated calomel reference electrode: +100 mV SCE), the rate of dissolution was faster than the diffusive transport, and accumulated dissolution products precipitated, forming a salt layer at the metal-solution interface. The resistance of this layer decreased the reaction rate by consuming the potential. Further increases in potential resulted only in increases in the thickness of the salt layer (usually about 100 Å [10 nm]); the current remained constant. Tester and Isaacs showed that the corrosion rate in this range of potential could be analyzed in terms of a diffusion-controlled process. After an initial transient period, the diffusion-controlled dissolution rate was slow enough to neglect moving boundary effects and a quasi-steady state was achieved where the current was shown to vary inversely with the square root of time.

Further experiments were conducted on stainless steel (Newman and Isaacs, 1983) in which the potential of an artificial pit undergoing dissolution in the diffusion-controlled region (+400 mV SCE) was switched to a lower potential (−100 mV SCE) at which the rate of diffusion was faster than the rate of dissolution. The salt layer dissolved within 1 s and the measured current slowly decreased (as the surface concentration of metal and chloride ions decreased and the metal surface became repassivated). During the repassivation process, the current decays rapidly following a short induction period. Using a transient mass transfer model, this current decline can be translated into a current-surface concentration plot. The shapes of these current-surface concentration curves indicate that several steady states may exist in the low-potential region in which the rates of diffusion and dissolution would balance. Thus multiple steady corrosion rates should be observed at the same applied potential, if the diffusion rate could be reduced further (by increasing the pit depth, for instance). In this study, an iron-base alloy, 304 stainless steel, and a nickel-base alloy, Alloy 600, were examined both to determine the rates of dissolution and diffusion, and to discover whether multiple corrosion rates could be observed.

Theory

Introduction

For any net electrochemical reaction to occur, a potential different from the thermodynamic equilibrium value is required. A qualitative relation between the current, as a measurement of the reaction rate, and the system overpotential is shown in Figure 1 (Albery, 1975; Vetter, 1967).

In region I, the activation-controlled region, the current is very low, and all of the overpotential is consumed at the alloy-solution interface. Both the voltage drop due to the solution resistance and the diffusion overpotential arising from limited mass transport rate to or from the fluid-metal interface are negligible. In this region, Tafel's law is valid and can be expressed as

$$\Delta E_{\text{total}} = \alpha \cdot \ln i + \ell \qquad (1)$$

where the constants α and ℓ depend on the reaction and on the reference electrode used.

As the overpotential increases outside of region I, the current or reaction rate increases exponentially, and the potential drop in the solution because of its resistance (the current-resistance, or IR drop) becomes increasingly important. The total overpo-

tential is then consumed by both the interfacial processes and the solution resistance. For this IR-controlled region, labeled region II in Figure 1, the following relation holds

$$\Delta E_{\text{total}} = \alpha \cdot \ln i + \beta + i \cdot R_s \qquad (2)$$

Further increase of overpotential may accelerate the reaction rate to the extent that the whole system becomes diffusion-controlled (region III). In chloride-activated pitting corrosion, this will result in the precipitation of a highly resistant salt layer at the electrode interface. The thickness of this salt layer (and thus its resistance) varies depending on the applied potential such that the extra voltage is consumed and the current is limited to the diffusion-controlled value. The current is then independent of the overpotential and is solely determined by the diffusional characteristics of the system (Tester and Isaacs, 1975).

In this work, a diffusion model of the artificial pit is used to determine the actual electrode surface concentration of ionic species as a function of time. This information is then used with experimental current-time data to determine the rates of reaction and diffusion in the pit for various electrode surface concentrations. The conditions for which the two rates are equal constitute the steady states of the system. Thus, experimental results together with an appropriate diffusion model will allow prediction of the steady state conditions.

The artificial pit geometry is cylindrical with nonreactive side walls, and the diffusion in the pit is one-dimensional with a heterogeneous reaction occurring at the bottom. However, several complications exist, such as the diffusion of several cations (mainly Fe^{2+}, Ni^{2+}, and Cr^{3+}), hydrolysis reactions of these ions, variable diffusivities of a particular ion due to the ionic concentration distribution in the pit, and the effect of applied potential gradient or current flow on ionic transport and concentration profiles (electromigration effect). Also, for shallow pits with high species flux, a hemispherical diffusion boundary layer may extend from the pit entrance into the bulk solution, and increase the actual diffusion length. Therefore, a considerable number of simplifications must be made to obtain a tractable physical model.

The first model simplification is to combine the effects of all of the reacting cations together into one hypothetical species, Me^{n+}. In the case of 304 stainless steel, this cation would be the molar average of the iron, nickel, and chromium present, having an average molecular weight 55.4, and an average valence 2.185. The solubility of this species is assumed to be that of $FeCl_2$, about 4.2 mol/L (Kuo and Landolt, 1974). The validity of this simplification can be partially verified by its utility in correctly predicting the relationship between the total coulombs passed through the system, and the resulting pit depth. The total coulombs per unit length of wire dissolved is given by:

$$Q = A \cdot \rho \cdot n \cdot F/M_w \qquad (3)$$

Using 1 mm dia. 304 stainless steel, for example, Eq. 3 reduces to $Q = 25.31$ C/mm depth.

The second simplification is that the extent of hydrolysis reactions in the pit is small, so that the concentration of H^+ can be neglected when compared to the concentration of Na^+ (approximately 1 mol/L). This assumption seems reasonable, since the hydrolysis equilibrium constant for the most hydrolyzed species, Cr^{3+}, is 10^{-4} mol/L. Assuming concentrations can be used for activities, the highest expected concentration of H^+ would be only 10^{-2} mol/L. This means that the only species to consider for possible electromigration effects are Me^{n+}, Na^+, and Cl^-. It should be noted that the pH of pit solutions in which the bulk solution was concentrated acid has been measured to be about 0.5 (Hakkarainen, 1981; Mankowski and Szklarska-Smialowska, 1975). In these highly acidic solutions, this assumption would not be valid.

Next, we assume that the diffusion length is simply the pit depth. The range of pit depths for which this assumption is valid can be determined from Figure 2, a plot of diffusion-limited current vs. inverse pit depth. An external hemispherical boundary layer would vary depending on the flux, making the relation nonlinear. Thus the assumption is valid over the linear range, or for pits deeper than about 0.4 mm. In this region, the current-pit depth product is a constant under diffusion-controlled steady state conditions.

The final assumption in our model is that the system can be characterized adequately by a single, constant effective diffusivity that takes into account the effects of variable diffusivity and electromigration. The error incurred from this approximation can be determined from the flux equation in Nernst-Einstein

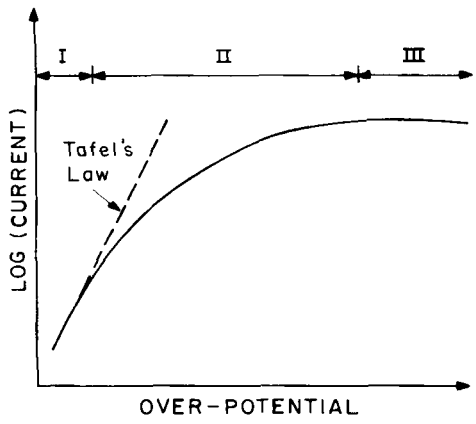

Figure 1. Regions of electrochemical reactions.
I, Activation-controlled region
II, IR-Controlled region
III, Diffusion-controlled region

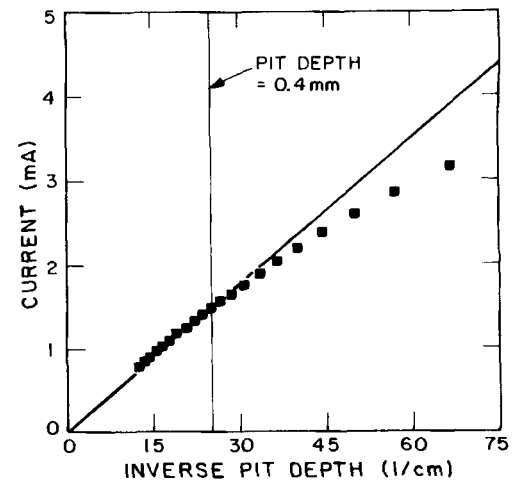

Figure 2. Diffusion-limited current vs. inverse pit depth.

form:

$$\frac{i}{nFA} = D_{me}\left[\frac{dC_{me}}{dx} + n \cdot C_{me}\frac{d\psi}{dx}\right] \tag{4}$$

This equation can be solved for constant or variable diffusivity,

$$D_{me} = D_o \quad \text{or} \quad D_{me} = \frac{D_o}{1 + b \cdot C_{me}} \tag{5}$$

with or without considering the electromigration effect (the second term on the righthand side of Eq. 4) (Galvele, 1976).

Figure 3 shows the relation between the electrode surface concentration and current-pit depth product, where the adjustable parameters D_o and b have been fitted to force the solution through both the origin and the constant current-pit depth product measured in Figure 2. Two important results can be seen in Figure 3. The first is that the effects of variable diffusivity and electromigration tend to counteract one another, so that the case in which both are considered is within 10% of the simplest case, that of a constant diffusivity. The second result is that the constant effective diffusivity fitted to our data is 0.824×10^{-5} cm^2/s (for 304 stainless steel). This is very close to the result quoted by Kuo and Landolt (1974) for $FeCl_2$ in water, of 0.85×10^{-5} cm^2/s.

Solution resistance corrections (IR drop)

The IR drop commonly refers to the system potential drop due to the electrical resistance of the solution. Because there is more solution in a deeper pit, the solution resistance will increase with increasing pit depth and will result in a larger potential drop. There will be less potential available for the electrode reaction in a deeper pit. To compare current decay curves measured at different pit depths, the solution resistance must be known in order to account for its effect.

The total potential drop in the system, ΔE_{total}, maintained by the potentiostat, is given by

$$\Delta E_{\text{total}} = \Delta E_W + \Delta E_{SCE} + \Delta E_{IR} \tag{6}$$

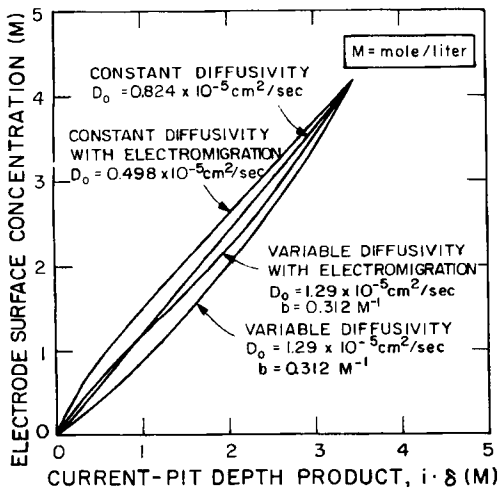

Figure 3. Effect of diffusion assumptions on electrode surface concentration.

The abscissa is normalized by dividing the current-depth product with $nFAD_o$ and is expressed in mol/L.

where ΔE_W and ΔE_{SCE} are the potential drops at the working electrode and at the saturated calomel electrode, respectively. ΔE_{IR} is the solution IR drop, and is related to the current through the system by Ohm's law:

$$\Delta E_{IR} = i \cdot R_s \tag{7}$$

The saturated calomel electrode is very stable and ΔE_{SCE} remains constant for all values of current under consideration. Therefore, for a given value of ΔE_{total}, the actual potential drop across the working electrode, ΔE_W, depends on the solution resistance R_s. For higher solution resistance, lower ΔE_W results.

The solution resistance in the pitting corrosion system consists of two parts: the resistance of the solution in the pit, and that of the bulk solution. The pit resistance, R_p, increases linearly with increasing pit depth, and the bulk resistance, R_b, is a constant. Theoretically, R_p and R_b are related to the specific resistance of the electrolyte solution, α, and to the system geometry by (Newman, 1974):

$$\begin{aligned} R_s &= R_p + R_b \\ &= \alpha\left(\frac{\delta}{\pi r^2}\right) + \alpha\left(\frac{1}{4r}\right) \\ &= (\text{constant})_1 \cdot \delta + (\text{constant})_2 \end{aligned} \tag{8}$$

A first approximation for R_s uses an approximate value of the specific resistance, α. From Robinson and Stokes (1959), the value of α for 1 mol/L NaCl solution at 25°C was measured to be 11.66 ohm · cm. With this value in Eq. 8, the total solution resistance was calculated to be

$$R_s(\text{ohm}) = 147.6 \cdot \delta(\text{mm}) + 58.3 \tag{9}$$

for a 1 mm dia. pit. The actual solution resistance used in the study was given by Eq. 8 with two experimentally determined constants.

The experimental method employed to determine the solution resistance was an application of the IR-controlled region discussed in the previous section. The electrode was first brought to a diffusion-controlled quasi-steady state by applying a high voltage (e.g., +400 mV SCE). The potential was then reduced to a value below the critical pitting value (e.g., −100 mV SCE) by a step change before again being raised to a high voltage. A typical current response during these step changes is shown in Figure 4.

At stage *A*, the system is diffusion-controlled with the surface salt layer present. Stage *B* exists at the lower voltage for less than a second. During this period the potential is low enough to reduce the reaction rate sufficiently to let the salt layer dissolve and diffuse away, while the time is short enough to keep the surface from becoming passivated. After switching back to high voltage, the activation-controlled reactions are fast and increase the solution concentration to a supersaturated level. The solution will continue to supersaturate until a point is reached at which spontaneous nucleation is initiated. At point *C*, the metal ion concentration reaches an unstable point and salt is precipitated. The sudden formation of a thick surface salt layer creates a large electrical resistance and lowers the current to point *D*. Finally, the salt layer dissolves to the proper thickness for the

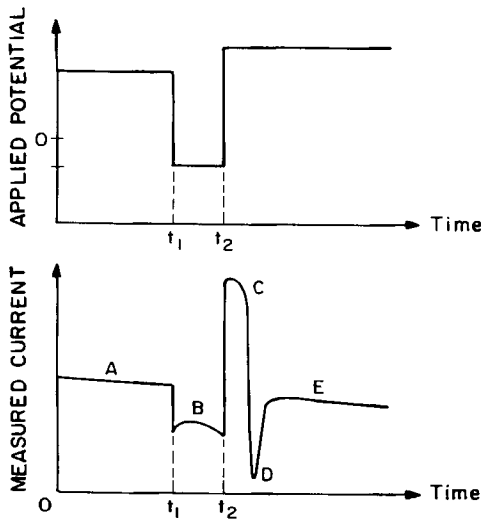

Figure 4. The IR drop measurement.

A, Diffusion-controlled quasisteady state
B, Removal of surface salt layer
C, Supersaturated solution of metal ions formed
D, Breakdown of supersaturation and sudden precipitation of surface salt layer
E, Diffusion-controlled quasisteady state

applied voltage, the current increases, and the whole system returns to steady state in the diffusion-controlled region (stage E).

At point C, there is no salt layer resistance and the current is so high that the reaction overpotential (the $\alpha \ln i$ term in Eq. 2) is approximately constant. The system is completely IR-controlled and Eq. 2 can be simplified to

$$\Delta E_{\text{total}} = i \cdot R_s + (\text{constant}) \tag{10}$$

A plot of ΔE_{total} vs. i at point C should yield a straight line with slope equal to R_s. The values of R_s obtained at different pit depths can be regressed to determine the two constants in Eq. 8.

All of the experiments used to construct the potential-current-surface concentration diagrams were conducted under conditions in which no surface salt layer exists. This is within region II of Figure 1 where both the IR drop and the reaction overpotential are important; Eq. 2 is valid. The measured current will depend on the solution resistance. For the same surface concentration and ΔE_{total}, the measured current i_1 at a given pit depth δ_1 (with resistance R_1) can be converted into the corresponding current i_2, which would have been observed if the pit depth had been δ_2 (with resistance R_2), by equating ΔE_{total} in Eq. 2 for each case:

$$i_1 \cdot R_1 + \alpha \cdot \ln i_1 = i_2 \cdot R_2 + \alpha \cdot \ln i_2 \tag{11}$$

where R_1 and R_2 are calculated using an empirical equation of the form of Eq. 8.

To use Eq. 11, the value of the Tafel's constant, α, must first be determined. It can be calculated by rearranging Eq. 2:

$$\Delta E_{\text{total}} - i \cdot R_s = \alpha \cdot \ln i + \text{const} \tag{12}$$

The lefthand side of Eq. 12 is the reaction overpotential, which is a characteristic only of the electrode reaction and is independent of pit depth. For a fixed surface concentration, the plot of $(\Delta E_{\text{total}} - i \cdot R_s)$ vs. $\ln i$ should yield a straight line with slope α. To locate a fixed surface concentration, we used the peak current of the transient decay curve in the linear regression. With the value of α. Equation 11 was solved for i_2.

Pit diffusion model

With the simplifications discussed above, it is possible to write the equations that govern the change in electrode surface concentration with time during our potential step experiments. The diffusion equation is:

$$\frac{\partial C_{me}}{\partial t} = D_{me} \frac{\partial^2 C_{me}}{\partial x^2} \tag{13}$$

Our experiments were started at the diffusion-limited current, so the initial condition is:

$$C_{me} = C_{sat} \cdot x/\delta \tag{14}$$

where $C_{sat} = 4.2$ mol/L, and the origin of the x axis is at the pit entrance. The boundary conditions are:

$$C_{me} = 0, \quad \text{at } x = 0$$

$$D_{me} \frac{\partial C_{me}}{\partial x} = \frac{i}{nFA}, \quad \text{at } x = \delta \tag{15}$$

In our experiments, the current underwent a transient response. The boundary condition is therefore time-dependent, experimentally determined, and no analytical solution is available, so a finite-difference numerical method was used. The initial condition (linear concentration profile) and the boundary conditions (experimental current) were discretized, and integrated with respect to time by Euler's method. The step size was reduced until the solution converged. Using this numerical solution, which gives the actual surface concentration as a function of time, we transformed the experimental current-time data into a plot of current (reaction rate) vs. surface concentration.

Location and stability of steady states

Figure 5 is an idealized diagram showing two isopotential lines on a graph of current density vs. surface concentration. As described in the preceding section, these lines give the rate of the surface dissolution reaction vs. electrode surface concentration at the given potential. The position of the isopotentials depends on the pit depth to which the curves have been IR-corrected. According to the surface flux equation developed above, Eq. 15, the diffusion rate can be represented as a straight line on this graph. This line passes through the origin and has a slope inversely proportional to the pit depth.

Point A is the diffusion-limited current. When the potential is suddenly switched so the current falls below the diffusion-controlled value a new current should be observed at either point B or point B', depending on the new potential. If the new imposed potential is low for the pit depth at which the experiment is conducted, curve $B'G$ describes the rate of surface reaction. In this case, the rate of surface reaction would be lower than the rate of diffusion at all values of electrode surface concentration. Thus

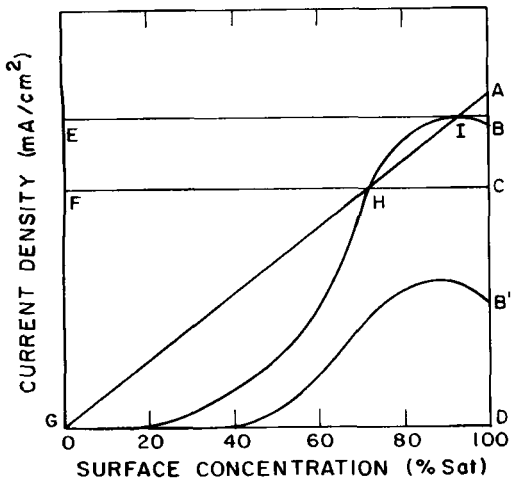

Figure 5. Theoretical prediction of multiple steady states.

the current would be observed to decay to zero as the surface became repassivated.

If, however, a high enough potential were imposed, curve *BIHG* describes the rate of surface reaction. In this case, the isopotential and diffusion lines cross, and there are three points (*G*, *H*, and *I*) where the rates of reaction and diffusion are equal. These are the predicted steady states. Alternatively, the pit depth could be increased, so that the slope of the diffusion line (*GA*) is decreased. By decreasing the diffusion rate sufficiently, the line would intersect reaction line *B'G*, and steady states at the lower potential would be found. With sufficient data these diagrams can be used to predict the lowest potential at which a steady state will be observed at a given pit depth (or, conversely, the shallowest pit depth for which a steady state will be observed upon step-changing to a given potential). They will also predict what the steady state currents will be for a given pit depth and potential.

The stability of the steady states can also be determined from the diagram. Stability is defined with respect to either potentiostatic conditions (in which all perturbations are along the isopotential *GHIB*) or with respect to galvanostatic (constant current) conditions (in which perturbations are along the constant current line *BE*, *CF*, or *DG*). Point *G* (the lower steady state) and point *I* (the upper steady state) are stable with respect to both potentiostatic and galvanostatic conditions. The steady state at point *H* (the intermediate steady state) is stable with respect to galvanostatic conditions, but unstable with respect to potentiostatic conditions. Thus the diagram predicts that a system held at point *H* under galvanostatic conditions will spontaneously move to either point *G* or point *I* if the system is suddenly switched to potentiostaic conditions.

Experimental Methods

Apparatus

The experimental apparatus is shown in Figure 6. The sample was a 1 mm dia. wire mounted in an inert epoxy plug and ground on grit paper to provide a smooth, flush surface at the beginning of the experiment. It was placed face upward in about 100 cm^3 of a 1 mol/L NaCl solution along with an auxiliary electrode and a reference, saturated calomel electrode (SCE). A potentiostat was used to set the potential across the system during the experiment, and the corresponding current vs. time was recorded on a strip chart. A digital coulometer was used to integrate the current continuously. The surface of the pit was monitored and photographed with a microscope.

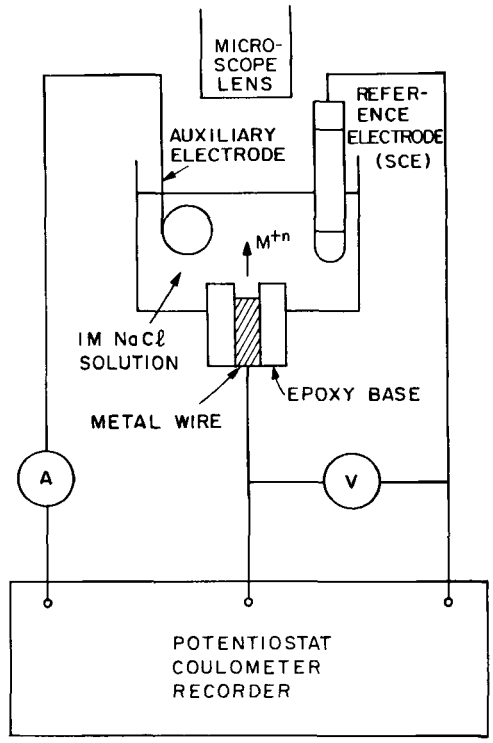

Figure 6. Experimental apparatus.

Artificial pit preparation

The metal surface was activated at the start of the experiment by applying a fixed potential of +400 mV SCE for 304 stainless steel and +600 mV SCE for Alloy 600, which were well above the critical pitting potential in 1 mol/L NaCl (about +100 and +250 mV SCE for 304 stainless steel and Alloy 600, respectively). The metal was allowed to dissolve until the desired pit depth was attained. The coulometer reading was used to determine the pit depth during the experiment by calculating the electricity required to dissolve a unit length of metal (see the Theory section). At the end of the experiment, a direct measurement of the pit depth was made with a micrometer. Measured and calculated depths agreed to within 1 to 2%.

Solution resistance (IR drop) measurement

The wire electrode was first activated above the critical pitting potential and the diffusion-controlled quasi-steady state was reached. The applied potential was then reduced to −100 mV SCE for 5 s to dissolve the surface salt layer. The system was again brought back to a high potential, ranging from 0 to +600 mV, SCE, to measure the transient current response. The system went through sequential stages of:

1. Supersaturation of metal ions
2. Precipitation of the surface salt layer
3. Resumption of the diffusion-controlled steady state.

The peak current at the supersaturation stage was recorded and used to determine the solution resistance.

Potential step experiments

The metal surface was activated at the start of an experiment. The metal was allowed to dissolve until the desired pit depth was attained. The coulometer reading was used to determine the pit depth during the experiments.

At the desired depth, the system was allowed to reach quasi-steady state. Then a potential step change was imposed on the system and the transient current response was recorded on a strip chart. The new imposed potential was below the critical pitting potential, so the current was observed to decay to zero (repassivation). The length of the response was dependent on the pit depth. The data from these experiments were used with the model developed above to predict the locations of the system steady states.

Experimental location of steady states

Two techniques were employed to experimentally locate the system steady states. The first technique was simply to conduct potential step experiments at increasing pit depths. For deep pits (greater than 0.8 mm for 304 stainless steel, for instance) the potential step did not result in transient repassivation where the current decays rapidly. Instead, a new steady state with a lower current density was achieved with the current decreasing at a slow rate as in the quasi-steady state before.

Experiments were then conducted at pit depths greater than the shallowest depth at which a potential step experiment resulted in a steady state. In these experiments a constant potential or a constant current was applied to the sample and the steady state value of the other was read. This allowed the observation of intermediate steady states that were stable only with respect to a constant imposed current.

Results

Solution resistance (IR drop)

The electrical resistance of the solution phase was determined by measuring the current at different applied potentials (0 to +600 mV SCE) in the IR-controlled region (at the supersaturation point as described in the experimental procedures). The total quantity of electricity passing through the system during one set of experiments was less than 0.8C. This corresponds to less than 0.03 mm increase in the pit depth, so an average pit depth was correlated with the measured resistance. When potential was plotted vs. current, all of these data sets yielded straight lines with correlation coefficients above 0.999, which shows the validity of assuming an average pit depth.

The solution resistance R_s is equal to the slope of the straight lines obtained above using 304 stainless steel wires. Figure 7 is the plot of solution resistance vs. pit depth. A linear relationship was obtained by regression

$$R_s(\text{ohm}) = (162.4 \pm 1.0) \cdot \delta(\text{mm}) + (44.8 \pm 8.4) \quad (16)$$

at 95% confidence level and with a correlation coefficient of 0.997. Also shown in Figure 7 is the theoretical resistance line for a 1 mol/L NaCl solution (Eq. 9). The agreement between the theory and the experimental data is very good for pit depths between 0.4 and 1.2 mm, where most of the potential step-change experiments were carried out. The agreement is probably fortuitous, since the complicating effects of high metal ion

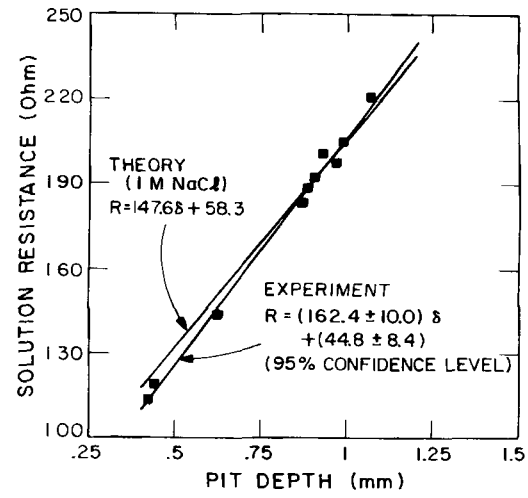

Figure 7. Comparison between theoretical and experimental correlations of solution resistance with pit depth.

concentration and steep concentration gradients in the pit would be expected to affect the slope of the resistance line.

The Tafel's constant a in the IR correction of Eq. 11 was determined by using Eq. 12. The experimental values of the current vs. the IR-corrected potential, which is the reaction overpotential ΔE-i R_s, are shown in Figure 8 as a semilog plot for the two alloys studied. The values of a were determined from linear regression to be 23.34 and 41.56 mV for 304 stainless steel and Alloy 600 wires, respectively. These fitted values of Tafel's constant for 304 stainless steel and Alloy 600 are in agreement with those measured in an earlier investigation at 23.9 and 38.9 mV, respectively.

Pit diffusion

Figure 9 shows the transient decay of current at various pit depths for potential step experiments conducted on 304 stainless steel. In all of these experiments the potential was switched at time zero from +400 to −100 mV SCE. Two features can be observed from this graph. First, the time required for the decay

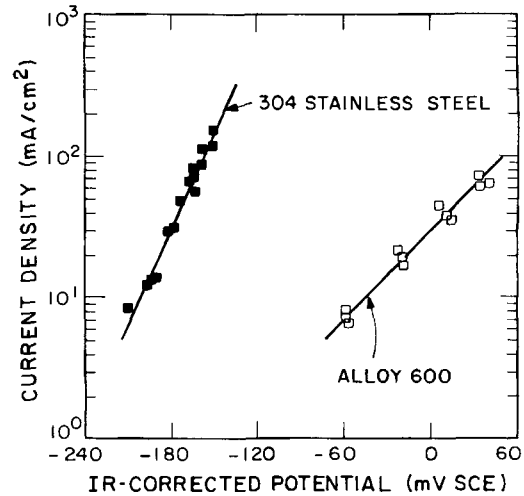

Figure 8. Determination of the Tafel's constant for 304 stainless steel and Alloy 600.

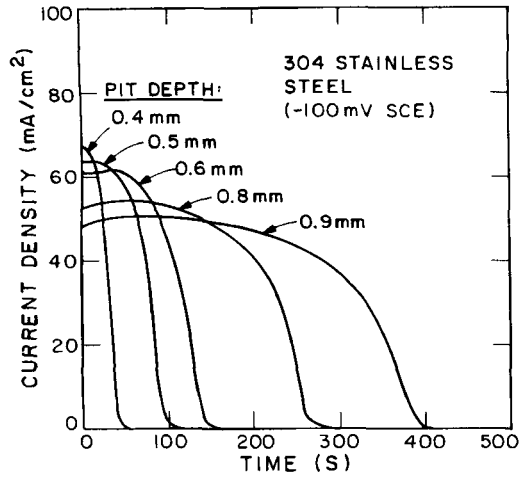

Figure 9. Experimental current-time decay curves at various pit depths for potential step change experiment.

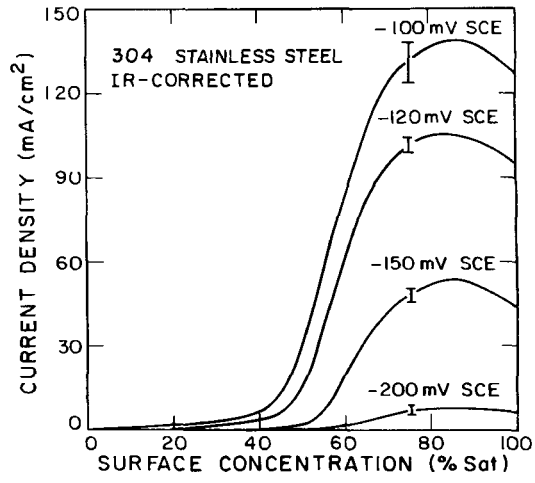

Figure 11. Reaction rates at different applied potentials for 304 stainless steel.

increases with increasing pit depth. This is consistent with the decay of current being caused by the diffusion of Me^{n+} away from the electrode surface and, therefore, by the reduction in Me^{n+} surface concentration after the step change in potential. The second observation is that the peak of the decay curve decreases with increasing pit depth. This is due to the increasing resistance of the solution in the pit, as described above.

Figure 10 shows the five experimental curves of Figure 9 after applying the transport model to determine the surface concentration as a function of time, and after correction for the solution IR drop to a hypothetical 0 mm pit depth. One noticeable feature in comparing Figures 9 and 10 is that the IR correction has not resulted in the same current density at high surface concentrations for data at different pit depths. Instead, the peak currents have been reversed, so that data at a depth of 0.9 mm have higher corrected currents than 0.8 mm, etc.

Aside from the peak reversal, the convergence of the curves is the expected result. With the diffusional and solution resistance effects accounted for, the isopotential line (in this case −100 mV SCE) can be obtained from the average of the curves. The resulting curve represents the "actual" surface kinetics by giving the rate of dissolution as a function of Me^{n+} surface concentration, although at slightly varying potentials (IR drops). The scatter between lines is a measure of our total error, including errors in experimental measurement and errors due to the use of a simplified diffusion model.

Accordingly, Figures 11 and 12, which present the results of our data reduction for 304 stainless steel and Alloy 600, contain error bars, which in each case is the standard deviation about the mean of a point-by-point averaging of curves from different pit depths. The largest error bar is about +7.5% of the peak value. If a 95% confidence limit on the mean is used for 20 points on each of the curves, an error bar of about ±2% results.

It should be noted that the resulting isopotential line can now be IR-corrected to any desired depth, since the result is exactly the same as independently correcting each of the curves at different pit depths to the desired depth and then averaging.

Steady states

Referring to our earlier discussion of Figure 5, the dynamics of the system can be studied by either increasing the applied

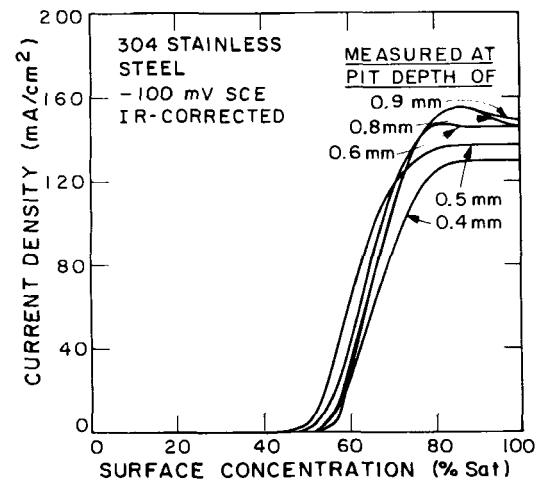

Figure 10. Experimental curves reduced with diffusion model and IR compensation.

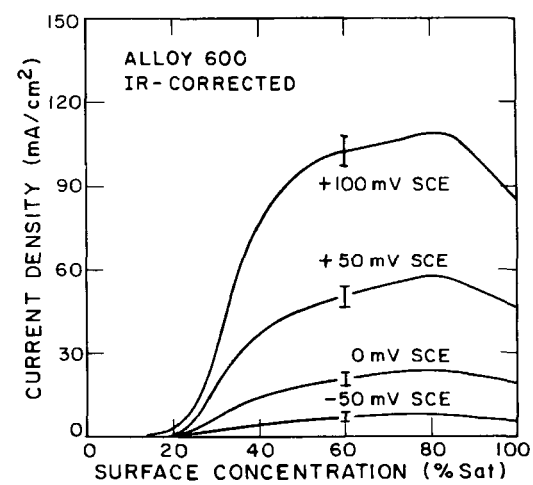

Figure 12. Reaction rates at different applied potentials for Alloy 600.

potential or by increasing the pit depth. By conducting experiments at pit depths larger than those where transient repassivation occurred, upper and intermediate steady states were observed for both 304 stainless steel and Alloy 600 at potentials below the critical pitting potential. As depicted by points *I* and *H* on Figure 5, surface concentrations should be below saturation with no salt film deposited. This was experimentally observed. For 304 stainless steel, a potential step change from +400 to −100 mV SCE resulted in a transient decay of current at a pit depth of 0.7 mm, but the same experiment resulted in a steady current of 61.8 mA/cm^2 at a pit depth of 0.8 mm. Further experiments were conducted at pit depths of 2.0 and 2.6 mm. In these experiments, the current was fixed and the potential was observed to achieve a steady value. For example, at 2.0 mm depth, and a fixed current of 11.1 mA/cm^2, the steady state potential observed was −127 mV SCE. When the mode of operation was switched to controlled potential at −127 mV SCE, the current slowly attained a new steady value of 27.5 mA/cm^2. These observations, as discussed earlier, indicate that the current densities above correspond to the intermediate (unstable with respect to potentiostatic conditions) and upper steady states, respectively, at −127 mV SCE and 2.0 mm pit depth. A similar experiment yielded upper and intermediate steady states of 21.2 and 9.6 mA/cm^2 at a potential of −147 mV SCE and a pit depth of 2.6 mm.

Experiments on Alloy 600 yielded an upper steady state at +100 mV SCE and a 1.4 mm pit depth with a current density of 52.4 mA/cm^2, and at +50 mV SCE and a 1.5 mm depth with a current density of 33.2 mA/cm^2. Upper and intermediate steady states of 29.3 and 13.8 mA/cm^2 were also found at +50 mV SCE and at a pit depth of 1.65 mm.

Throughout these experiments, whenever the galvanostatically stable intermediate state was switched to the potentiostatic condition, it always went to the more activated upper steady state. No complete repassivation was observed.

Discussion

By using a simplified one-dimensional transient diffusion model with current-resistance (IR) corrections for different pit depths, we were able to predict the relationship between corrosion current density for 304 stainless steel and Alloy 600 as a function of the concentration of metal chloride at the active metal surface. Furthermore, the results can be used generally to predict the repassivation behavior of the system at any pit depth. Depending on the size of the applied voltage, the magnitude of the current density varied widely. At all applied potentials, the current density was much lower for Alloy 600 in comparison to 304 stainless steel for experiments conducted at room temperature (25°C) and in an initially 1 mol/L NaCl aqueous environment. However, 304 stainless steel repassivated at higher surface metal chloride concentrations. An idealized corrosion-resistant alloy for this environment would need to combine the properties of both stainless steel and Alloy 600.

A major contribution to the analysis of the transient anodic current behavior under stepped voltage conditions was the observation and prediction of the existence of multiple steady states. These were seen at surface metal chloride concentrations below saturation where the normal quasi-steady state diffusion-controlled current behavior exists at applied voltages larger than the pitting potential. Both unstable and stable steady states were experimentally identified for 304 stainless steel and Alloy 600. For example, an upper stable steady state and intermediate unstable steady state were observed for Alloy 600 at +50 mV SCE at a pit depth of 1.65 mm. The current densities and fractional surface concentrations were 29.3 mA/cm^2 at 58.5% of saturation for the upper steady state and 13.8 mA/cm^2 at 28.0% of saturation for the intermediate steady state. This is in contrast to the diffusion-controlled dissolution rate of 49.2 mA/cm^2 observed under quasi-steady state conditions with a 100% saturated surface concentration of metal chlorides present.

As seen in Figure 12, these fractional concentrations are in the region where one might expect to find these steady states. The current density maximum of 60 mA/cm^2 from the +50 mV SCE curve on Figure 12 can be corrected for the IR drop to a 1.65 mm depth using Eq. 11 with α = 41.6 mV and R_s from Figure 7. This reduces the peak current density to 24.0 mA/cm^2, which should correspond to the steady state reaction rate observed. However, the prediction is 22% lower than the experimental value. Similar calculations for other observed steady states in Alloy 600 and 304 stainless steel also show predicted upper steady states 20 to 30% lower than observed. Given the above discrepancies, either the diffusion or corrosion rate was inaccurately predicted or extrapolated, or some basic new mechanism became more important during the steady state experiment than during normal transient repassivation, since we can predict the latter behavior correctly. First one should note that the steady state experiments involved longer times and deeper pits than the transient repassivation tests. Given that the predicted diffusion rate could be matched to the repassivation behavior and that the surface concentrations predicted are reasonable, the corrosion rate will be underpredicted since the observed upper steady state current density was greater than the estimated value. The reversal of the current density peaks for different pit depths that occurred when the data of Figure 9 were IR-corrected and replotted in Figure 10, may indicate the possibility of an incorrect Tafel slope or solution resistance resulting in inaccurate compensation of IR drop, particularly for the deeper pits. Also, microscopic examination of the wire electrode surface before and during dissolution indicated the presence of significant surface roughening during the steady state experiments as compared to a smooth, uniformly dissolving surface in the quasi-steady diffusion-controlled regime. This effect would tend to increase the calculated current density based on the nominal cross-sectional area of the wire because the actual dissolving surface area is larger. Although surface roughening was observed microscopically only with samples that were maintained at low applied potential or low constant current for more than 30 min, nonuniform pitting was clearly initiated much earlier but was not visible under the low-power magnification of the microscope used.

The experimental facts suggest that both solution resistivity effects and microscopic surface area changes could explain the discrepancies between the observed and predicted steady state points. It is likely that both mechanisms may be important in this system.

Acknowledgment

The research was conducted at the Brookhaven Station of the MIT School of Chemical Engineering Practice and was funded by the Brookhaven National Laboratory under the auspices of the Office of Basic Energy Studies of the U.S. Department of Energy, Division of Materials Science, under Contract No. DE-AC02-76-CH00016.

Notations

A = wire cross-sectional area, cm^2
α = Tafel's constant, mV
β = experimentally determined constant, mV
b = concentration dependence parameter of diffusivity, L/mol
C = concentration, mol/L
C_{me} = metal ion concentration, mol/L
C_{sat} = saturated metal ion concentration, mol/L
D = diffusivity, cm^2/s
D_{me} = metal ion effective diffusivity, cm^2/s
D_o = infinite dilution diffusivity, cm^2/s
E = potential, mV
ΔE_{total} = total system potential drop, mV
ΔE_{SCE} = saturated calomel electrode potential drop, mV
ΔE_{IR} = solution potential drop, mV
ΔE_W = working electrode potential drop, mV
F = Faraday's constant, 96,500 C/equiv
i = current, mA
M_w = avg. molecular weight, g/mol
n = avg metal valence, equiv/mol
Q = total electricity
R = electrical resistance, ohm; gas constant 8.314 J/mol · K
R_b = bulk solution resistance, ohm
R_p = pit solution resistance, ohm
R_s = total solution resistance, ohm
r = wire radius, cm
T = temperature, K
t = time, s
x = pit length, coordinate, cm

Greek letters

α = solution specific resistance, ohm · cm
δ = total pit depth, cm
ϕ = potential driving force for electromigration, V
ρ = avg. metal density, g/cm^3
ψ = dimensionless potential, $= F\phi/RT$

Literature Cited

Albery, J., *Electrode Kinetics,* Clarendon, Oxford, pp. 12–15 (1975).

Beck, T. R., "Pitting of Titanium. II: One-dimensional Pit Experiments," *J. Electrochem. Soc.,* **120,** 1,317 (1973).

Galvele, J. R., "Transport Processes and the Mechanism of Pitting of Metals," *J. Electrochem. Soc.,* **123**(4), 464 (1976).

Hakkarainen, T., "The Growth of Corrosion Pits in Austenitic Steel," *Proc. 8th Int. Cong. Metallic Corrosion,* DECHEMA, (1981).

Kuo, H. C., and D. Landolt, "Rotating Disc Electrode Study of Anodic Dissolution of Iron in Concentrated Chloride Media," *Electrochem. Acta,* **20**(5), 393 (1974).

Mankowski, J., and Z. Szklaraska-Smialowska, "Studies of Accumulation of Chloride Ions in Pits Growing During Anodic Polarization," *Corrosion Sci.,* **15,** 493 (1975).

Newman, J., "Mass Transport and Potential Distribution in the Geometrics of Localized Corrosion," *Proc. U. R. Evans Int. Conf. Localized Corrosion, Nat. Assoc. Corrosion Eng.,* Houston (1974).

Newman, R. C., and H. S. Isaacs, "Dissolution and Passivation Kinetics of Fe-Cr-Ni Alloys During Localized Corrosion," *Proc. 5th Int. Symp. Passivity, Passivity of Metals and Semi-Conductors,* Elsevier, Amsterdam (1983).

Robinson, R. A., and R. H. Stokes, *Electrolyte Solutions,* 2nd ed., Butterworths, London (1959).

Tester, J. W., and H. S. Isaacs, "Diffusional Effects in Simulated Localized Corrosion," *J. Electrochem. Soc.,* **122**(11), 1,438 (1975).

Vetter, K. J., *Electrochemical Kinetics,* Academic Pr., New York, p. 119 (1967).

Manuscript received Jan. 28, 1985, and revision received Nov. 1, 1985.